Journal of Maps

ISSN: (Print) (Online) Journal homepage: www.tandfonline.com/journals/tjom20

High-resolution bathymetry coupled with 3D models of hydrothermal vents from opportunistically-acquired imagery: Aurora vent field, Arctic Ocean

Tea Isler, Michael Jakuba, Tom Kwasnitschka, Autun Purser, Andrew Klesh, Vera Schlindwein & Christopher R. German

To cite this article: Tea Isler, Michael Jakuba, Tom Kwasnitschka, Autun Purser, Andrew Klesh, Vera Schlindwein & Christopher R. German (2024) High-resolution bathymetry coupled with 3D models of hydrothermal vents from opportunistically-acquired imagery: Aurora vent field, Arctic Ocean, Journal of Maps, 20:1, 2404878, DOI: 10.1080/17445647.2024.2404878

To link to this article: https://doi.org/10.1080/17445647.2024.2404878

JOURNAL OF MAPS
2024, VOL. 20, NO. 1, 2404878
https://doi.org/10.1080/17445647.2024.2404878

SCIENCE

OPEN ACCESS Check for updates

High-resolution bathymetry coupled with 3D models of hydrothermal vents from opportunistically-acquired imagery: Aurora vent field, Arctic Ocean

Tea Isler [a,b], Michael Jakuba [c], Tom Kwasnitschka [d], Autun Purser [a], Andrew Klesh[e], Vera Schlindwein [a,b] and Christopher R. German [c]

[a]Alfred Wegener Helmholtz Centre for Polar and Marine Research, Bremerhaven, Germany; [b]University of Bremen, Bremen, Germany; [c]Woods Hole Oceanographic Institution, Woods Hole, Massachusetts, USA; [d]GEOMAR Helmholtz Centre for Ocean Research Kiel, Kiel, Germany; [e]Jet Propulsion Laboratory, California Institute of Technology, Pasadena, California, USA

ABSTRACT

Active venting at the Aurora hydrothermal field was first located in 2014. In July 2023, the AUV/ROV Nereid Under Ice (NUI) expanded the known size of the Aurora hydrothermal field, discovering 7 'black smokers' together with associated lower-temperature flow. In this study, we present a new high-resolution bathymetric map acquired from NUI which has allowed us to identify morphological features previously undetectable from ship multibeam. All known active vents are aligned along a single 230 m-long ridge, parallel to the Gakkel Ridge strike direction and intersected by a scarp following the general trend of the Lena Trough. The new vents were measured at up to 17 m height from 3D models generated using structure-from-motion techniques applied to opportunistically acquired imaging data collected while in exploration mode. The extent of extinct sulfides present, together with the towering height of vents are consistent with a period of sustained high-temperature venting at Aurora.

ARTICLE HISTORY
Received 26 July 2024
Revised 7 September 2024
Accepted 10 September 2024

KEYWORDS
Underwater photogrammetry; hydrothermal vents; geomorphology; ultraslow ridges; 3D reconstruction

1. Introduction

Deep-sea hydrothermal vents, first discovered in 1977 during the Southtow and Pleiades expeditions to the Galapagos Rift (Corliss et al., 1979), revealed the presence of abundant microorganisms living in extreme environments. Two years later, in 1979, higher temperature vents, commonly known as 'black smokers', were discovered at the East Pacific Rise (Spiess et al., 1980). Until the mid-1990s a common assumption was that such high-temperature hydrothermal vents should primarily be found along fast-spreading ridges, following the theory correlating the abundance of venting to the ridge spreading rate (Baker et al., 1996). That global vent distributions might be more complex became recognized later that decade with the location of higher incidences of venting than anticipated along both the slow-spreading Mid-Atlantic Ridge (German et al., 1996) and the ultra-slow spreading SW Indian Ridge (German et al., 1998). These findings were further consolidated in 2001 when evidence of abundant sources of hydrothermal venting was reported from the Gakkel ridge in the Arctic Ocean (Baker et al., 2004; Edmonds et al., 2003). Because of the remoteness of the Gakkel ridge, however, it was not until 2014 that our team was able to return to the westernmost (hence, most accessible) of the hydrothermal source locations identified by Edmonds et al. (2003) and determine the precise location of seafloor venting at the Aurora hydrothermal field. During that expedition, onboard the *RV Polarstern* (Alfred-Wegener-Institut Helmholtz-Zentrum für Polar – und Meeresforschung, 2017), extensive water column and seafloor video surveys were conducted culminating in imaging of 'black smoker' venting with the OFOS deep-tow camera system (Boetius, 2015).

1.1. Aurora vent field, Gakkel ridge

Ultra-slow spreading ridges are considered distinct from all other classes of mid-ocean ridge, consisting of both magma-rich and magma-starved accretionary ridge segments (Dick et al., 2003). On the Gakkel Ridge, where transform offsets are largely absent, this diversity in spreading mode is particularly distinct (Michael et al., 2003) with the Western Volcanic Zone (WVZ: 7°W-3°E) and the Eastern Volcanic Zone (EVZ: 29°E-85°E) separated by the Sparsely Magmatic Zone (SMZ: 3°E-29°E). The Aurora seamount is situated near 6°W at a depth of 3800 m and with an elevation of ~150 m above the seafloor, close to the western limit of the WVZ where the rift valley curves

CONTACT Tea Isler tea.isler@awi.de Van Ronzelen Strasse 2, 27568 Bremerhaven, Germany
Supplemental data for this article can be accessed online at https://doi.org/10.1080/17445647.2024.2404878

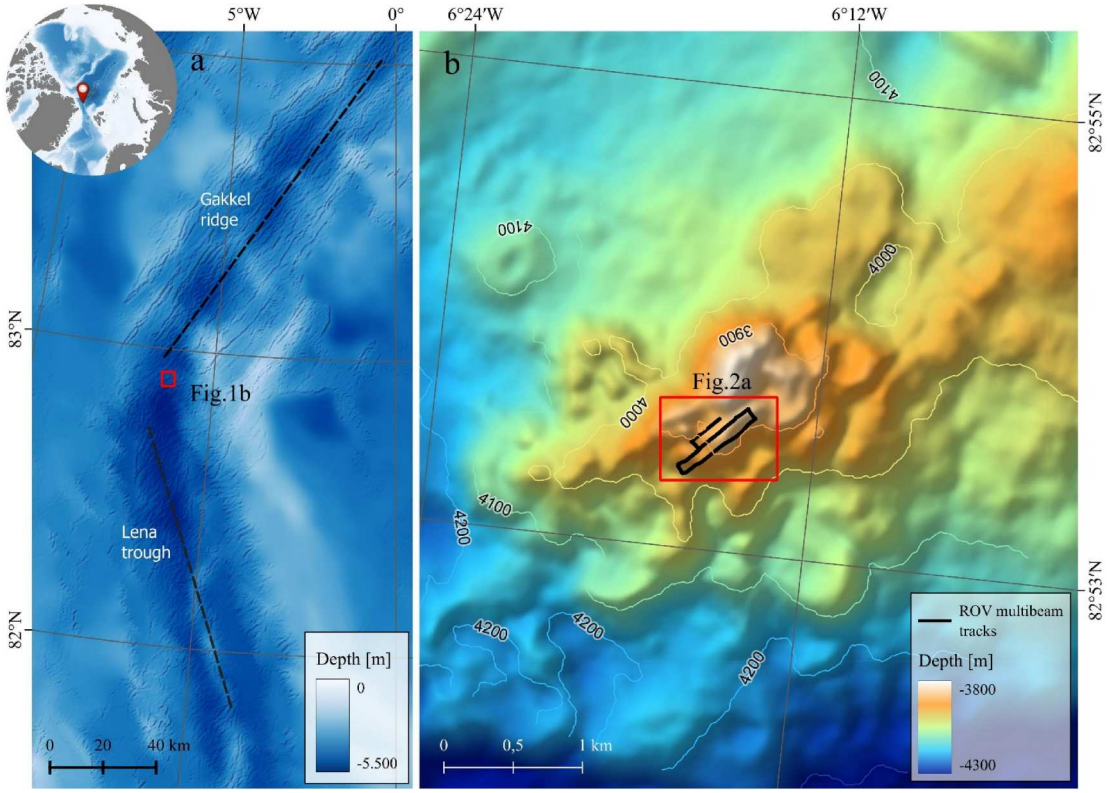

Figure 1. Location of the Aurora vent field. The dashed lines in (a) reflect the regional trends of the Gakkel Ridge and Lena Trough, as derived from GEBCO 2023 bathymetry (200 m resolution); (b) shows the track lines for the mapping survey carried out by the AUV/ROV NUI during expedition PS137 (2023) overlain on the 20 m-grid bathymetry collected from *RV Kronprins Håkon* in 2019 (Bünz et al., 2020). The depth labels indicate the maximum and minimum depths.

into the northern end of the Lena Trough (Figure 1). The WMZ, generally, is characterized by volcanic ridges with morphologies reminiscent of more magmatically robust, faster-spreading ridges (Michael et al., 2003). Indeed, dredging at Aurora in 2001 recovered only basaltic rocks together with extinct polymetallic sulfide material (Edmonds et al., 2003). However, hydrothermal plume studies at Aurora subsequently led to predictions of ultramafic influence upon seafloor venting at this location (German et al., 2022). In late 2021, the first remotely operated vehicle (ROV) expedition confirmed the location identified in 2014 by naming three distinct 'black smokers'. Those vents (named *Enceladus*, *Ganymede* and *Hans Torre Vent [HTV]*) are all located within 5–10 m of each other, and approximately 500 m southwest and downslope from the seamount's summit (Boetius, 2015; Ramirez-Llodra et al., 2023). In July 2023, seven additional 'black smoker' vents and an abundance of lower-temperature seafloor fluid flow were discovered, extending from ~80 m to 130 m further SW from the already known vents (Schlindwein, 2023; Jakuba et al., [in press]).

A motivation for this project, therefore, has been to provide a deeper understanding of the distribution of venting at the Aurora site and the relationship of that venting to seafloor setting in as much detail as possible. Because of the remoteness of the site and the limited time available for seafloor operations on each dive, however, a key challenge has been to maximize the amount of information that could be extracted from opportunistically acquired images collected while in ROV exploration mode. To achieve this, we have employed a non-invasive technique known as structure-from-motion which uses multiple images to generate a textured 3D model of the observed scene (Kwasnitschka et al., 2013).

1.2. Structure-from-motion

The use of structure-from-motion photogrammetry techniques in underwater studies has been extensively explored, as reviewed generally by Hu et al. (2023) and Song et al. (2022), and has been applied in fields such as seafloor habitat mapping (de Oliveira et al., 2021; Price et al., 2019) and marine archaeology (Drap et al., 2015; Johnson-Roberson et al., 2017; Menna et al., 2018). Photogrammetry has also been previously applied to hydrothermal vents but in those cases, dedicated ROV dives with purposely planned trajectories were conducted to allow for high-resolution reconstructions across sub-centimeter length scales (Boittiaux et al., 2023; Gerdes et al., 2019; Van Audenhaege et al., 2024). In contrast, the approach presented here achieves geological reconstruction of the seafloor area at the outcrop scale (order 1–100 m).

Furthermore, past structure-from-motion surveys with carefully planned trajectories were only possible by revisiting vent locations that had already been well characterized (Boittiaux et al., 2023; Gerdes et al., 2019). Here, instead, we show that a first reconstruction of a hydrothermal field is possible using data collected while the ROV is still in exploration mode. By preserving the verticality of tall hydrothermal vents, 3D models allow us to conduct further investigations (e.g. habitat mapping) which would otherwise not be possible using classic multibeam technologies (Robert et al., 2017). The scaled 3D model of the new hydrothermal vents is presented in this study and coupled with a new high-resolution bathymetric map covering the hydrothermally active Aurora site. In combination, these approaches allow us to achieve morphological characterization of this vent site at a higher resolution than was previously possible, providing a more complete understanding of the geological processes active within the study area and for new scientific hypotheses to be developed.

2. Methods

During the course of the exploration at Aurora in July 2023, 3 dives (043, 044 and 045) were carried out by the NUI vehicle (Bowen et al., 2014; Jakuba et al., 2018; Jakuba et al., 2024) in both autonomous mode, during mapping operations, and remotely operated mode, during bottom time, as summarized in Table 1 and illustrated in Figure 2. The switch between the two modes was possible as a tether fiber connected the vehicle to the ship, allowing for the pilot to directly drive the vehicle or be augmented through autonomous operations during the entirety of all dives.

2.1. Vehicle navigation

NUI was equipped with an INS system iXBlue Phins III 6000 paired with a Doppler Velocity Log (DVL) TRDI Workhorse Navigator 300 kHz and a Paroscientific Digiquartz depth sensor to provide the precise ROV navigation tracks for all near-seafloor operations shown in Figure 2. Due to difficulties with the USBL (ultra-short baseline) system onboard the *RV Polarstern*, the absolute positioning of these tracks was achieved by identifying the precise location of the Hans Tore Vent (HTV) which was unambiguously recognizable from the memorial stone deployed in 2021 during the HACON21 expedition (Ramirez-Llodra et al., 2023). This same vent, with its distinct 'sunken crater' morphology, was first named during the HACON19 expedition (Bünz et al., 2020) where USBL navigation confirmed that it lay to within ±5 m of where the first imaging of 'black smoker' venting was observed in 2014 (Boetius, 2015).

Table 1. Summary of the dives carried out by NUI at the Aurora vent field. Dives 043 and 044 consisted of camera surveys only, combined with sample collection. Dive 045 conducted a high-resolution mapping survey before descending to the seafloor.

Dive	Max Depth	Total Time	Bottom Time	Ship Drift	Max Separation (ship to NUI)
043	3901 m	09:50	02:14 camera survey (ROV)	3300 m	1500 m
044	3922 m	09:23	03:21 camera survey (ROV)	4100 m	2100 m
045	3970 m	09:35	02:16 camera survey (ROV) 01:34 seabed mapping (AUV)	3300 m	1400 m

2.2. Sonar data acquisition and processing

The multibeam echosounder (MBES) data was collected using the Norbit WBMS 400kHz multibeam sonar installed at the rear end of the NUI vehicle. The mapping survey carried out during dive 045 at Aurora acquired three parallel transects of data collected at a constant altitude of ~30 m with a swath coverage of 160° (Figure 2). Corrections for sound velocity were applied during the data acquisition process using the sound velocity probe installed on the NUI vehicle. The raw MBES data was processed in CARIS HIPS&SIPS adjusting for attitude offsets and outliers. The final point cloud was gridded at 1 m resolution using the swath angle weighting method in CARIS.

2.3. Imagery acquisition

For this expedition, the vehicle was equipped with multiple cameras of which only two provided colored high-resolution images, suitable for 3D reconstruction purposes: (1) a fixed-mount Rayfin HDE-GigE-6000-DBH13-LO (1920 × 1080 pixels) camera, and (2) a pan and tilt zoom Kongsberg OE14-522FS-0009 (1280 × 720 pixels) camera. Of the three dives carried out at Aurora, only two (dives 044 and 045) provided sufficiently high-quality images, free of turbidity, for photogrammetric purposes. By contrast, the first dive (043) was focused on the relocation of the already known vents (HTV, Enceladus, Ganymede) followed by sampling at the low-temperature *Dragonfly* vent, adjacent to HTV. Throughout this dive, the vehicle was either stationary, or surrounded by turbid water (from sulfide resuspension and or hydrothermal 'black smoke'). By contrast, the next two dives (044 and 045) were carried out at newly discovered vent sites where landing and take-off were free from smoke or sediment resuspension. Although producing good quality images used in the 3D reconstruction, dive 044 also prioritized vent-fluid sampling resulting in multiple duplicate images when the vehicle was stationary at the seabed. Dive 045 produced a more

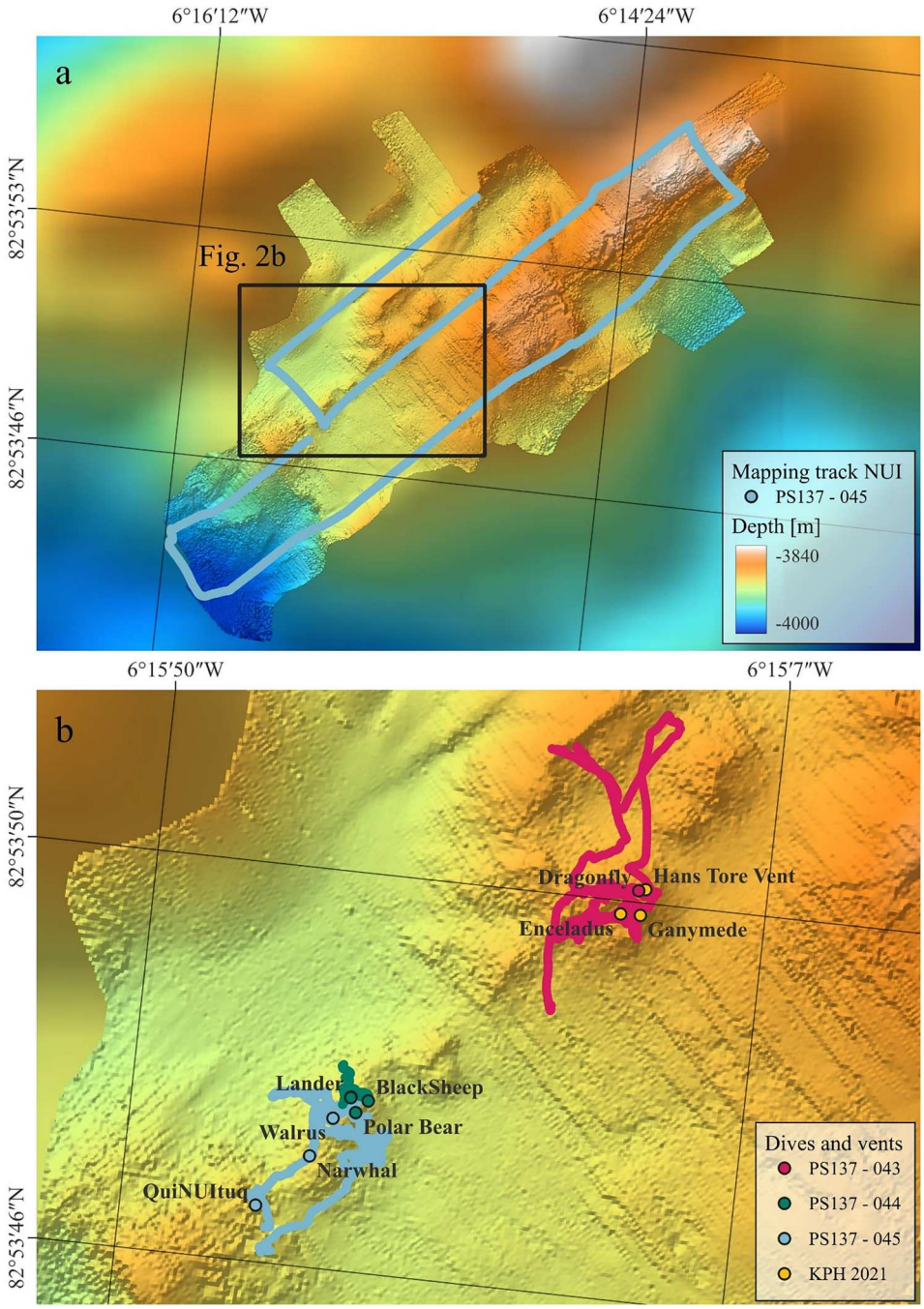

Figure 2. (a) High-resolution bathymetric map covering the full extent of the known Aurora hydrothermal field, with survey track-lines overlain. NUI was set to mapping mode with a constant speed and altitude, while conducting the multibeam survey. (b) Track-lines for NUI on-bottom exploration and sampling operations, during which the vehicle was pilot-controlled, remotely, using a fiber-optic micro-tether for communications. All vent locations are color-coded according to the dives on which they were first encountered. Background ship's multibeam bathymetry map is from HACON19 (Bünz et al., 2020). The depth labels indicate the maximum and minimum depths.

heterogeneous and high-quality image dataset while conducting a systematic search for new vents, examining previously unexplored features of the freshly mapped seafloor. Even so, visual contact with the seafloor was lost multiple times while flying across unfamiliar and very uneven terrain, either due to flying too far off-bottom or through dense plumes of mineral smoke that obscured the field of view. For each camera, one frame per second was extracted from the two dives producing more than 20,000 frames covering the newly-extended Aurora hydrothermal field.

2.4. Image processing and 3D reconstruction

The steps followed for the 3D reconstruction from the opportunistic data collected in exploratory mode can be categorized into 2 stages: preparation and reconstruction. The first, preparation, required both data cleaning and formatting, in which images were

clustered into groups consisting of sequences of seafloor-visible frames and then contrast correction using the Contrast Limited Adaptive Histogram Equalization (CLAHE) algorithm (Pizer et al., 1987). Next, reconstruction was performed using *Agisoft Metashape* software. General guidelines are outlined in the User's Manual v. 2.0 (Agisoft Metashape, 2023) and have previously been applied in multiple marine environment studies (Pierce et al., 2021), (Wang et al., 2024). The key steps followed for reconstruction, in this study, were: (1) an alignment process applied to each individual clustered group of images, (2) the merging of discrete clusters of images using manually placed markers assigned to distinct and recognizable features, and (3) the generation of 3D textured mesh models of the combined dataset.

Traditionally, in underwater studies, reconstructed models can be scaled based on known measurements such as the distance between laser points installed on the vehicle (Price et al., 2019), by the distance between reference objects placed on the seafloor (Wang et al., 2024), or by using the distance between aligned georeferenced frames (Ferrera et al., 2023; Gerdes et al., 2019). In this opportunistic study, we relied on the known distance between the two cameras, measured at 29.3 cm, on deck. The *Supplementary Material 1* (SM1) file contains more information on the approach followed in this study.

3. Results

3.1. Morphology from high-resolution bathymetry

The high-resolution bathymetric map gridded at 1 m and extending for 700 m along the ridge axis, covers all known active hydrothermal vents identified from the Aurora hydrothermal field, to-date (Figure 3). The most striking observation is that all the discovered vents at Aurora, are spaced along a linear, ~10 m tall ridge which runs from North East to South West across the surveyed area. Known active venting extends over a distance of 135 m, but the ridge itself measures 230 m in length, extending beyond the sites of identified venting by 55 m to the NE and 40 m to the SW: regions that have never, yet, been visually investigated. Notably, this hydrothermally active ridge could not be resolved previously from ship-based multibeam bathymetry. At its southwest limit, this ridge is truncated by a scarp that is orthogonal to the strike of the hydrothermally active ridge and offsets the depth of the seafloor to south and west with a drop of more than 10 m. This is also apparent in the larger-scale terraced structure of the entire Aurora seamount (Figure 2).

Examining the high-resolution bathymetry away from the sites of active venting, multiple elongated depressions parallel to the orientation of the major scarp are visible in the central area of the map (Figure 3). These features vary in size with lengths of up to 60 m, maximum widths of 4 m and depths of ~3 m. The distance between such depressions ranges from ~4 to 10 m. We can be confident that these structures are not artifacts of our multibeam data processing because these same 'trench-like' features were also observed, recurrently, during camera surveys conducted aboard the RV Polarstern in 2014. Figure 4 shows two examples of this in which a steep-sided trench cuts through thickly layered sediments. In some instances, filter feeding glass sponges were observed at the deepest point of these trenches.

3.2. 3D Reconstruction

Of the 20,000 frames available, more than 15,000 had to be removed during the first stage of processing described previously, due to poor visibility in the field of view and/or duplication of images during sampling times when NUI was stationary at the seafloor. Due to motion-related blurriness and illumination flashes, only 3300 of the remaining 5000 images were used to reconstruct 6 of the new high-temperature vents discovered in 2023.

The newly discovered vents vary in shape and height. The first tall vent observed, Polar Bear, is composed of 2 vertical edifices emerging from a single thick sulfide base reaching a height of almost 10 m above the seafloor. This was the only vent that could be entirely reconstructed in 3D, because good-quality images were taken from multiple angles all around this structure (Figure 5 right). A second taller 'black smoker', the QuiNUItuq, located at the southwestern end of the area explored, exhibits a similar structure to Polar Bear but reaches a height of 17 m (Figure 5 left). Due to the limited bottom time available, a sufficient survey could not be completed around QuiNUItuq, which was limited to the southern face of the vent only.

The section of ridge-crest that hosts the Polar Bear structure also contains 4 additional high-temperature 'black smoker' vents and associated low-temperature venting within an area of $\leq$80 m^2, and exhibiting heights that range between 0.3 and 2 m tall. Two additional tall edifices were imaged in the vicinity of the black smokers at *Black Sheep* (Figure 2(b)) but because NUI did not approach close enough for detailed visual inspection, it was not possible to establish whether those chimneys were currently hydrothermally active or already extinct. The surrounding surveyed area, all along the crest of the new vents, was characterized by fallen chimneys up to 2 m long and more broken and blockier brightly colored mineralization.

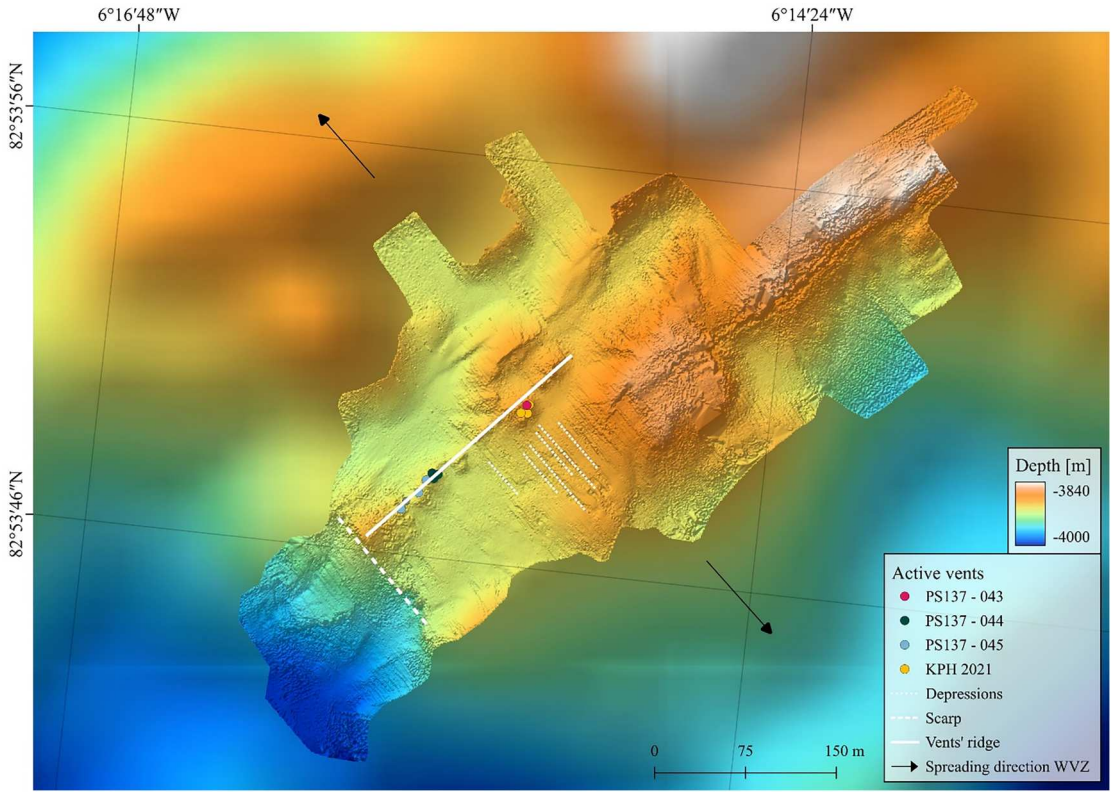

Figure 3. High-resolution bathymetry collected during PS137. All known active vents are closely aligned and are located on the crest of a ~230 m long ridge which is aligned sub-parallel to the general NE-SW strike of the Gakkel Ridge. Black arrows show the regional-scale spreading direction of the Gakkel Ridge WVZ (See Figure 1). The depth labels indicate the maximum and minimum depths.

4. Discussion

This first reconstruction of the Aurora vent field aims to provide a comprehensive map of this topographically complex environment which allows for a better understanding of the spatial distribution and scales of the newly discovered hydrothermal vents (Figure 6).

The close alignment of all ten active 'black smoker' vents over a distance of 135 m is larger than is typical among volcanically-hosted vent systems on a slow-spreading ridge such as the Mid-Atlantic Ridge, and closer in size to those controlled by tectonism (German et al., 2016). In that work, it was also noted that among the few active sites of venting yet located along any ultra-slow ridge, anomalously large hydrothermal fields have been reported independent of their style of geologic (neo-volcanic vs. tectonics dominated) setting. At Aurora, the presence of a linear array of vents along a topographic high, aligned closely to the spreading direction could be considered consistent with neovolcanic influence. Given that the Aurora field sits at the intersection of the WVZ of the Gakkel Ridge and the cross-cutting orientation of the Lena Trough, we might expect that the geologic controls of venting at this hydrothermal field might be complex. For example, the heights and breadths of the tallest chimneys, together with the large volume of sulfides present and the absence of any extrusive volcanic rocks exposed at the seafloor close to the vents, all point to a long period (kyr) of sustained high-temperature venting. An alternative hypothesis, therefore, could be that the elongated nature of the Aurora hydrothermal field results from multiple sites of upflow aligned with some subsurface fault plane. In that case, the linear topographic high upon which all the currently active vents sit could be due to mineral precipitation and accumulation on an otherwise relatively flat seafloor, as is seen immediately to either side (Figure 3). A second observation backing the theory of the vents' self-made ridge is the morphological difference between such ridge and the more scarp-controlled ridge, immediately adjacent to the NW, and from the large ridge feature off-set to the SE where the highest elevations of the surveyed area are reached. Whichever may be the case, the high ratio of CH4:Mn concentrations in hydrothermal plume samples, certainly indicates that seawater must be penetrating deep enough to interact with ultramafic lithologies somewhere beneath the seafloor at Aurora (German et al., 2022).

The new 3D reconstruction obtained from the high-resolution multibeam bathymetry also allows us to pose other geological questions. For example, is the large scarp cutting across the mapped region

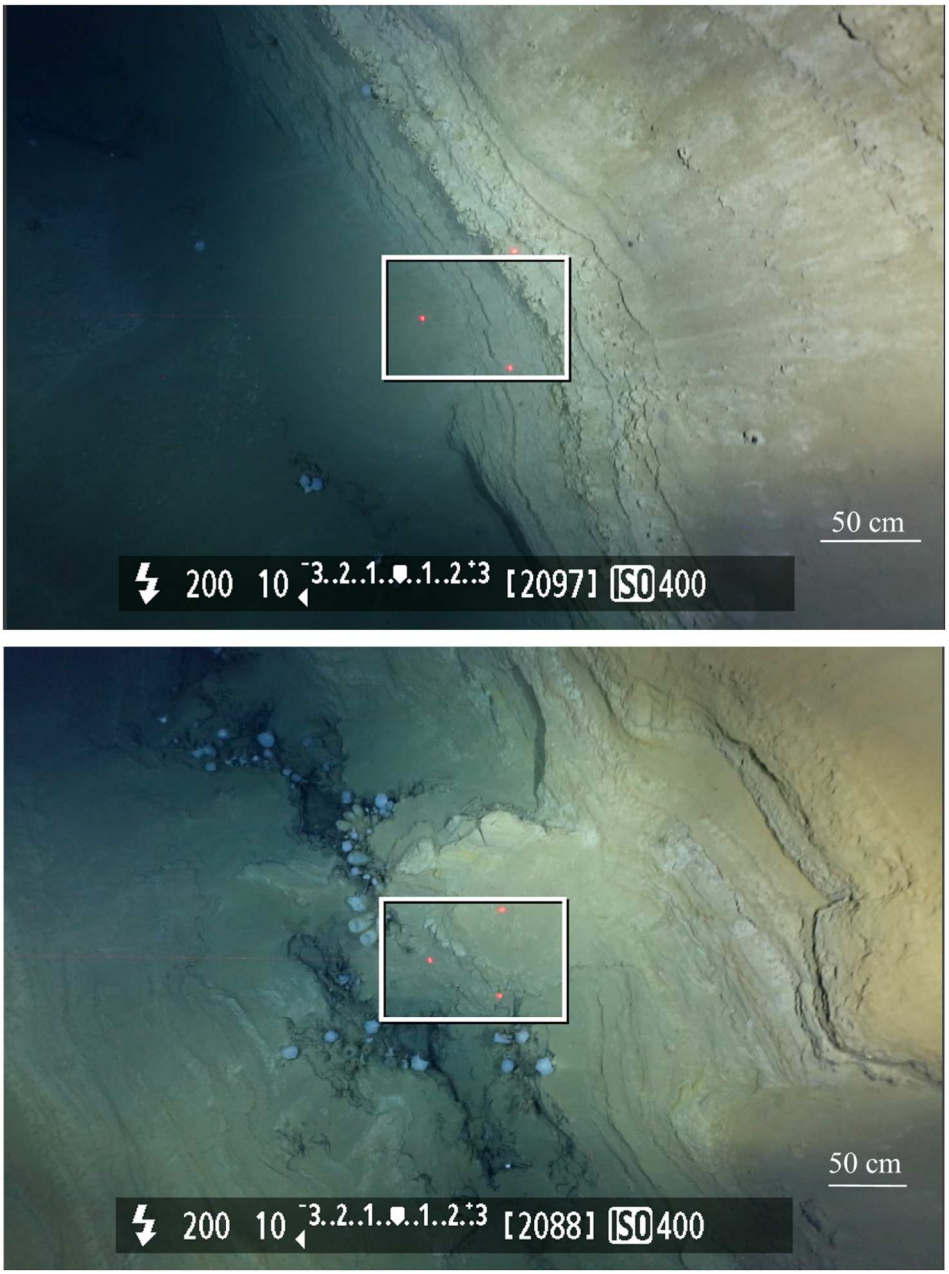

Figure 4. Elongated depressions of the same dimensions and orientation as observed in the high-resolution bathymetry survey (Figure 3) have also been observed, visually, during seafloor camera surveys, adjacent to sites of active venting at Aurora (Boetius, 2015). Note the thick layering of sediments within the walls of each trench-like depression and the concentrations of glass sponge filter feeders visible at their base.

generated from faulting of the lithosphere (in an orientation sub-parallel to the alignment of the Lena Trough) or, conversely, might it reflect successive terminations of lava flows emanating from the summit of the Aurora seamount? Without further seafloor ground-truthing to characterize key geologic relationships, determining the chronological interplay of tectonic faulting and episodes of extrusive volcanism remains elusive. Thus, the high-resolution map of Aurora presented here, coupled with 3D reconstructions of the newly discovered hydrothermal vents, provides the opportunity to identify gaps in knowledge, develop new hypotheses and prioritize key areas for future exploration. While previous structure-from-motion underwater studies have focussed on the fine-scale details of 3D models constructed across limited spatial scales, our approach has revealed a practical ability to combine dedicated high-resolution mapping with the use of structure-from-motion, drawing upon opportunistically collected camera images. The Main Map offers a clear progression from a high-level overview of the area to a detailed 3D visualization of individual vents at the Aurora vent field. This was particularly valuable work to undertake for our Arctic seafloor surveys, in such a logistically inaccessible, remote and ice-covered location. However, the approach followed and demonstrated in this study, should be equally applicable

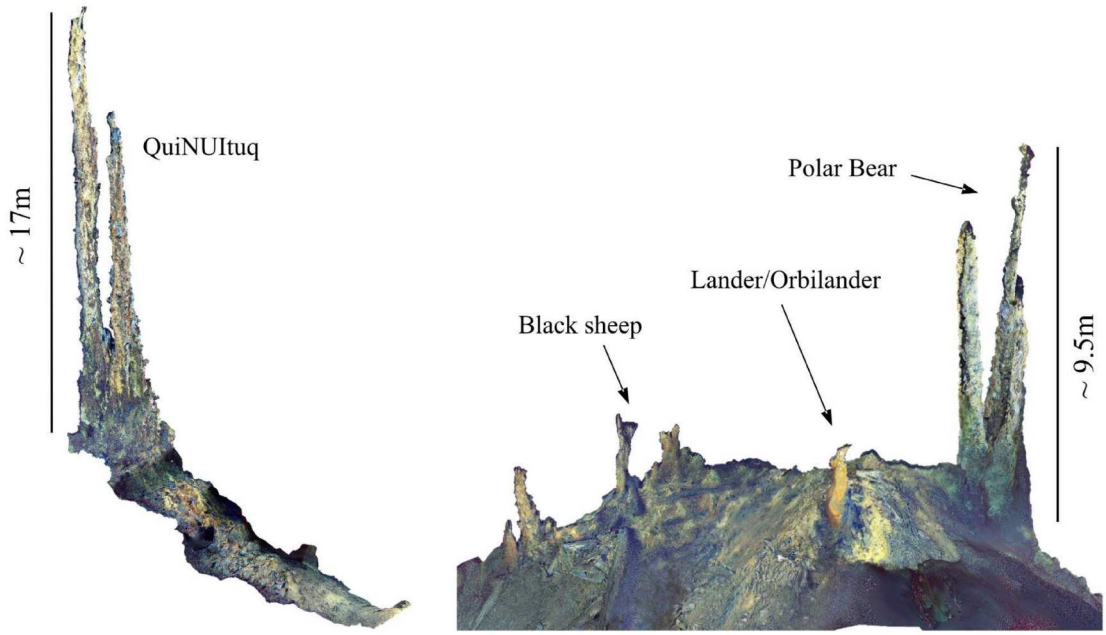

Figure 5. Snippets of the textured 3D model of the newly discovered vents. The tallest vent, *QuiNUItuq* (left) and *Polar Bear*, *Black sheep* and *Lander/Orbilander* (right).

wherever exploration-mode ROV operations are conducted, wherever images and multibeam bathymetry are (or already have been) collected (Liang et al., 2023; Salinas-de-León et al., 2018). Available photogrammetric software already provide detailed instructions on the acquisition of optical data for 3D reconstruction purposes. In the *Supplementary Material 2* file (SM2) we provide our recommendations for future implementation, informed by the challenges encountered while undertaking this work. Those guidelines could improve the quality of opportunistically-acquired images which, in turn, could allow for faster 3D reconstructions to be performed while simultaneously reducing uncertainties (Ferrera et al., 2023). In the current study, however, we have demonstrated how 3D models can be obtained from opportunistic data, where cameras are used as navigation instruments.

The creation of 3D models of regions of deep ocean seafloor, wherever possible, do not just allow us to investigate already-visited regions in greater detail to better constrain the complex processes in play. They also provide a readily accessible medium for increasing public and scientific awareness of the diverse environments found several thousand meters below the ocean surface, helping to inform and inspire where humanity should explore next.

5. Conclusions

In this study, we have combined a new high-resolution bathymetric map of the Aurora hydrothermal field in the Arctic Ocean with opportunistically acquired imagery to generate a scaled 3D model of areas of active seafloor venting. Our work facilitates a better understanding of the detailed geomorphological setting of the vent-sites at a level of detail far superior to what was possible with previously available ship-based bathymetric maps. These new surveys allow for visualization over length scales comparable to the outcrop-scale investigations that could traditionally only be undertaken by land-based geologists. Small ridges, scarps and elongated depressions following directions that are both parallel and orthogonal to the general orientation of the Gakkel Ridge are resolvable across the ~160,000 m^2 area mapped in this study. Of particular note, the scaled 3D reconstruction generated from our opportunistically acquired data has allowed us to reveal that all ten 'black smoker' hydrothermal vents at Aurora, together with abundant areas of lower-temperature venting, are all aligned along a single ~ 230 m topographic feature. This study, when combined with complementary geochemical analyses of the source hydrothermal fluids that are still underway, will provide us with new insights into, and develop novel hypotheses concerning, the geologic controls on the Aurora hydrothermal field.

Software and data availability

The MBES data from the ROV was processed in *CARIS HIPS and SIPS* v11.4.29.

Python v3.9.19 was used to extract the frames from the video recordings and apply the CLAHE contrast correction. The 3D models of the vents were reconstructed using *Agisoft Metashape 2.0* and run on an Intel Core i7 processor with 64 GB of RAM and an NVIDIA RTX A1000 GPU with 2048 CUDA cores.

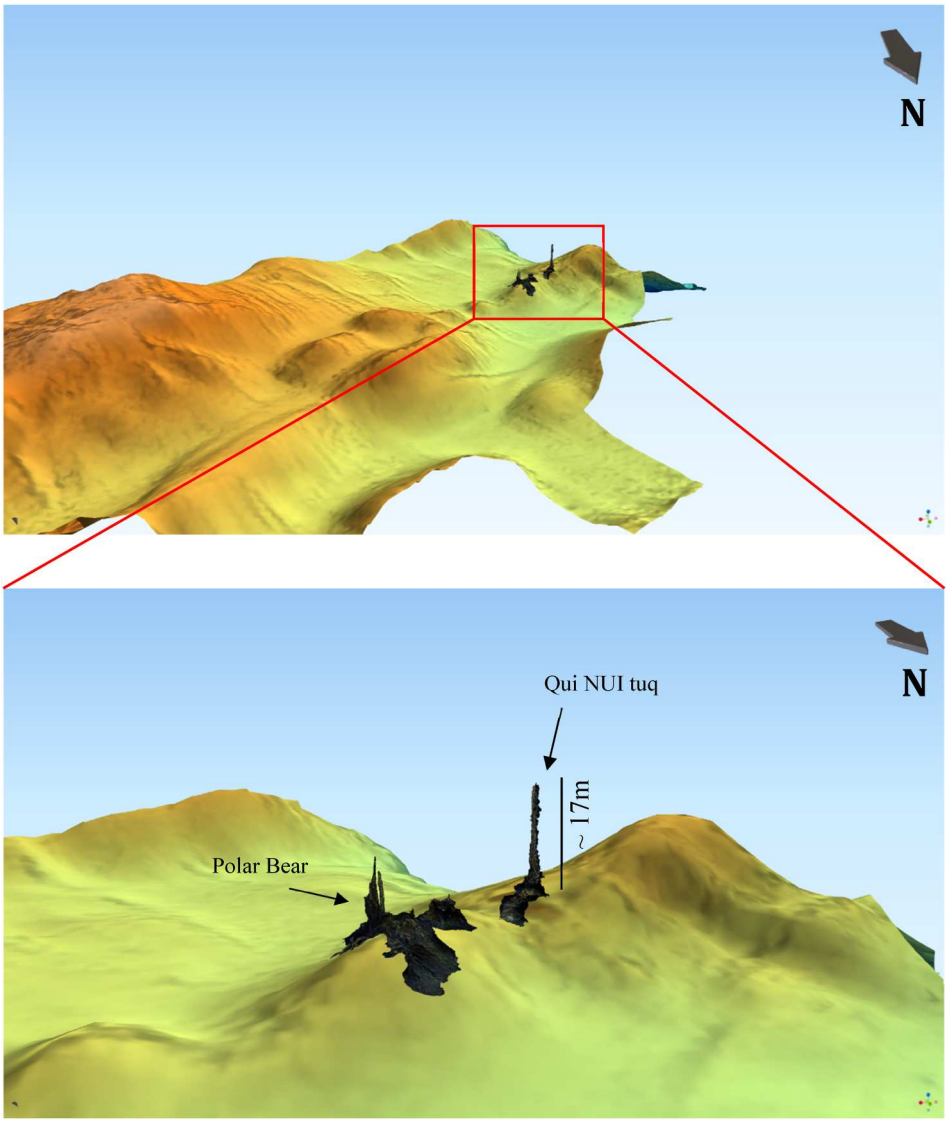

Figure 6. 3D models of the recently discovered vents placed on the 1 m high-resolution bathymetry from PS137. The color scheme of the bathymetry is the same as in Figures 2 and 3.

All maps were created in QGIS v3.32.1, including the 3D view of Figure 6 where the *Qgis2threejs* plugin was used.

All video recordings from PS86 are available in PANGAEA (doi.pangaea.de/10.1594/PANGAEA.839397).

The standard definition (SD) resolution videos from the Rayfin camera of the NUI dives 044 and 045 are available in PANGAEA (https://doi.pangaea.de/10.1594/PANGAEA.971306; https://doi.pangaea.de/10.1594/PANGAEA.971307). The original higher resolution videos can be requested from Christopher German.

Acknowledgements

The authors thank the crew and scientific team onboard Polarstern during expedition PS137. Particularly, the whole NUI engineering team is acknowledged for providing the expertise to complete such a challenging but rewarding field program and for the technical support provided during all post-cruise data processing. TI thanks POLMAR for the funding to pursue a short-term research stay at WHOI, which allowed to advance and finalize the proposed manuscript.

Disclosure statement

No potential conflict of interest was reported by the authors.

Funding

The Polarstern PS137 Cruise was funded through grant number AWI_PS137_04, in Germany. In the USA, participation of the NUI team, from both WHOI and JPL, was supported by NASA Astrobiology Program PSTAR Award: 80NSSC22K1312. CRG also acknowledges additional support from NASA Astrobiology Program Award 80NSSC19K1427. TI received support from the Nippon Foundation-GEBCO Seabed 2030 Project.

ORCID

Tea Isler http://orcid.org/0009-0001-1805-6702
Michael Jakuba http://orcid.org/0000-0002-0440-0074

Tom Kwasnitschka http://orcid.org/0000-0003-1046-1604
Autun Purser http://orcid.org/0000-0001-5427-0151
Vera Schlindwein http://orcid.org/0000-0001-5570-2753
Christopher R. German http://orcid.org/0000-0002-3417-6413

References

Agisoft Metashape (Version 2.0). (2023). https://www.agisoft.com/.

Alfred-Wegener-Institut Helmholtz-Zentrum für Polar- und Meeresforschung. (2017). Polar research and supply vessel POLARSTERN operated by the Alfred-Wegener-Institute. *Journal of Large-Scale Research Facilities JLSRF*, *3*(3), A119. https://doi.org/10.17815/jlsrf-3-163.

Baker, E. T., Chen, Y. J., & Morgan, J. P. (1996). The relationship between near-axis hydrothermal cooling and the spreading rate of mid-ocean ridges. *Earth and Planetary Science Letters*, *142*(1-2), 137–145. https://doi.org/10.1016/0012-821X(96)00097-0

Baker, E. T., Edmonds, H. N., Michael, P. J., Bach, W., Dick, H. J., Snow, J. E., Walker, S. L., Banerjee, N. R., & Langmuir, C. H. (2004). Hydrothermal venting in magma deserts: The ultraslow-spreading Gakkel and Southwest Indian Ridges. *Geochemistry, Geophysics, Geosystems*, *5*(8), Q08002. https://doi.org/10.1029/2004GC000712.

Boetius, A. (2015). The expedition PS86 of the research vessel POLARSTERN to the Arctic ocean in 2014. *Alfred-Wegener-Institut, Helmholtz-Zentrum für Polar- und Meeresforschung. In Berichte zur Polar- und Meeresforschung = Reports on Polar and Marine Research*, *685*, 1–133. https://doi.org/10.2312/BzPM_0685_2015

Boittiaux, C., Dune, C., Ferrera, M., Arnaubec, A., Marxer, R., Matabos, M., Van Audenhaege, L., & Hugel, V. (2023). Eiffel tower: A deep-sea underwater dataset for long-term visual localization. *The International Journal of Robotics Research*, *42*(9), 689–699. https://doi.org/10.1177/02783649231177322

Bowen, A. D., Yoerger, D. R., German, C. C., Kinsey, J. C., Jakuba, M. V., Gomez-Ibanez, D., Taylor, C. L., Machado, C., Howland, J. C., & Kaiser, C. L. (2014). Design of Nereid-UI: A remotely operated underwater vehicle for oceanographic access under ice. In *2014 Oceans - St. John's,* St. John's, NL, Canada (pp. 1–6). IEEE.

Bünz, S., Ramirez-Llodra, E., German, C., Ferre, B., Sert, F., Kalenickenko, D., Reeves, E., Hand, K., Dahle, H., & Kutti, T. (2020). RV Kronprins Håkon (cruise no. 2019708) Longyearbyen–Longyearbyen 19.09.–16.10. 2019. https://haconfrinatek.com/2020/01/20/hacon-cruise-report/f.

Corliss, J. B., Dymond, J., Gordon, L. I., Edmond, J. M., von Herzen, R. P., Ballard, R. D., Green, K., Williams, D., Bainbridge, A., & Crane, K. (1979). Submarine thermal springs on the Galápagos Rift. *Science*, *203*(4385), 1073–1083. https://doi.org/10.1126/science.203.4385.1073

de Oliveira, L. M. C., Lim, A., Conti, L. A., & Wheeler, A. J. (2021). 3D classification of cold-water coral reefs: A comparison of classification techniques for 3D reconstructions of cold-water coral reefs and seabed. *Frontiers in Marine Science*, *8*, 640713. https://doi.org/10.3389/fmars.2021.640713

Dick, H. J., Lin, J., & Schouten, H. (2003). An ultraslow-spreading class of ocean ridge. *Nature*, *426*(6965), 405–412. https://doi.org/10.1038/nature02128

Drap, P., Seinturier, J., Hijazi, B., Merad, D., Boi, J.-M., Chemisky, B., Seguin, E., & Long, L. (2015). The ROV 3D project: Deep-sea underwater survey using photogrammetry: Applications for underwater archaeology. *Journal on Computing and Cultural Heritage*, *8*(4), 1–24. https://doi.org/10.1145/2757283

Edmonds, H. N., Michael, P. J., Baker, E. T., Connelly, D. P., Snow, J. E., Langmuir, C. H., Dick, H. J. B., Mühe, R., German, C. R., & Graham, D. W. (2003). Discovery of abundant hydrothermal venting on the ultraslow-spreading Gakkel ridge in the Arctic ocean. *Nature*, *421*(6920), 252–256. https://doi.org/10.1038/nature01351

Ferrera, M., Arnaubec, A., Boittiaux, C., Larroche, I., & Opderbecke, J. (2023). Vision-based 3D reconstruction for deep-Sea environments: Practical Use for surveys and inspection. In *OCEANS 2023 - Limerick*, Limerick, Ireland (pp. 1–7). IEEE. https://doi.org/10.1109/OCEANSLimerick52467.2023.10244338

Gerdes, K., Martínez Arbizu, P., Schwarz-Schampera, U., Schwentner, M., & Kihara, T. C. (2019). Detailed mapping of hydrothermal vent fauna: A 3D reconstruction approach based on video imagery. *Frontiers in Marine Science*, *6*, 96. https://doi.org/10.3389/fmars.2019.00096

German, C., Baker, E., Mevel, C., Tamaki, K., & Team, F. S. (1998). Hydrothermal activity along the southwest Indian ridge. *Nature*, *395*(6701), 490–493. https://doi.org/10.1038/26730

German, C., Klinkhammer, G. P., & Rudnicki, M. (1996). The rainbow hydrothermal plume, 36°15′N, MAR. *Geophysical Research Letters*, *23*(21), 2979–2982. https://doi.org/10.1029/96GL02883

German, C. R., Petersen, S., & Hannington, M. D. (2016). Hydrothermal exploration of mid-ocean ridges: Where might the largest sulfide deposits be forming? *Chemical Geology*, *420*, 114–126. https://doi.org/10.1016/j.chemgeo.2015.11.006

German, C. R., Reeves, E. P., Türke, A., Diehl, A., Albers, E., Bach, W., Purser, A., Ramalho, S. P., Suman, S., Mertens, C., Walter, M., Ramirez-Llodra, E., Schlindwein, V., Bünz, S., & Boetius, A. (2022). Volcanically hosted venting with indications of ultramafic influence at Aurora hydrothermal field on Gakkel Ridge. *Nature Communications*, *13*(1), 6517. https://doi.org/10.1038/s41467-022-34014-0

Hu, K., Wang, T., Shen, C., Weng, C., Zhou, F., Xia, M., & Weng, L. (2023). Overview of underwater 3D reconstruction technology based on optical images. *Journal of Marine Science and Engineering*, *11*(5), 949 https://doi.org/10.3390/jmse11050949.

Jakuba, M. V., Curran, M., Nakilcki, V., Isler, T., Klesh, A., Buenger, H. J., Dalpe, A., Lindzey, L., Silvia, M., Loer, R., German, C. R., & The PS137 engineering & science team (2024). Exploring the aurora vent field: 4000 m under ice with the NUI hybrid remotely operated vehicle [in press]. In *2024 IEEE OES autonomous underwater vehicle symposium (AUV)*.

Jakuba, M. V., German, C. R., Bowen, A. D., Whitcomb, L. L., Hand, K., Branch, A., Chien, S., & McFarland, C. (2018). Teleoperation and robotics under ice: Implications for planetary exploration. In *2018 IEEE aerospace conference* (pp. 1–14). IEEE. https://doi.org/10.1109/AERO.2018.8396587

Johnson-Roberson, M., Bryson, M., Friedman, A., Pizarro, O., Troni, G., Ozog, P., & Henderson, J. C. (2017). High-resolution underwater robotic vision-based mapping and three-dimensional reconstruction for

archaeology. *Journal of Field Robotics*, *34*(4), 625–643. https://doi.org/10.1002/rob.21658

Kwasnitschka, T., Hansteen, T. H., Devey, C. W., & Kutterolf, S. (2013). Doing fieldwork on the seafloor: Photogrammetric techniques to yield 3D visual models from ROV video. *Computers & Geosciences*, *52*, 218–226. https://doi.org/10.1016/j.cageo.2012.10.008

Liang, J., Tao, C., Zheng, Y., Zhang, G., Su, C., Yang, W., Liao, S., & Wang, N. (2023). Geology context, vent morphology, and sulfide paragenesis of the longqi-1 modern seafloor hydrothermal system on the ultraslow-spreading southwest Indian ridge. *Deep Sea Research Part I: Oceanographic Research Papers*, *194*, 103962. https://doi.org/10.1016/j.dsr.2023.103962

Menna, F., Agrafiotis, P., & Georgopoulos, A. (2018). State of the art and applications in archaeological underwater 3D recording and mapping. *Journal of Cultural Heritage*, *33*, 231–248. https://doi.org/10.1016/j.culher.2018.02.017

Michael, P. J., Langmuir, C. H., Dick, H. J. B., Snow, J. E., Goldstein, S. L., Graham, D. W., Lehnert, K., Kurras, G., Jokat, W., Mühe, R., & Edmonds, H. N. (2003). Magmatic and amagmatic seafloor generation at the ultraslow-spreading gakkel ridge, Arctic ocean. *Nature*, *423*(6943), 956–961. https://doi.org/10.1038/nature01704

Pierce, J., Butler, I. V., Rzhanov, M. J., Lowell, Y., Dijkstra, K., & A, J. (2021). Classifying 3-D models of coral reefs using structure-from-motion and multi-view semantic segmentation. *Frontiers in Marine Science*, *8*, 706674. https://doi.org/10.3389/fmars.2021.706674

Pizer, S. M., Amburn, E. P., Austin, J. D., Cromartie, R., Geselowitz, A., Greer, T., ter Haar Romeny, B., Zimmerman, J. B., & Zuiderveld, K. (1987). Adaptive histogram equalization and its variations. *Computer Vision, Graphics, and Image Processing*, *39*(3), 355–368. https://doi.org/10.1016/S0734-189X(87)80186-X

Price, D. M., Robert, K., Callaway, A., Lo Lacono, C., Hall, R. A., & Huvenne, V. A. I. (2019). Using 3D photogrammetry from ROV video to quantify cold-water coral reef structural complexity and investigate its influence on biodiversity and community assemblage. *Coral Reefs*, *38*(5), 1007–1021. https://doi.org/10.1007/s00338-019-01827-3

Ramirez-Llodra, E., Argentino, C., Baker, M., Boetius, A., Costa, C., Dahle, H., Denny, E. M., Dessandier, P.-A., Eilertsen, M. H., & Ferre, B. (2023). Hot vents beneath an icy ocean. *Oceanography*, *36*(1), 6–17. https://doi.org/10.5670/oceanog.2023.103

Robert, K., Huvenne, V. A. I., Georgiopoulou, A., Jones, D. O. B., Marsh, L., Carter, G. D. O., & Chaumillon, L. (2017). New approaches to high-resolution mapping of marine vertical structures. *Scientific Reports*, *7*(1), 9005. https://doi.org/10.1038/s41598-017-09382-z

Salinas-de-León, P., Phillips, B., Ebert, D., Shivji, M., Cerutti-Pereyra, F., Ruck, C., Fisher, C. R., & Marsh, L. (2018). Deep-sea hydrothermal vents as natural egg-case incubators at the Galapagos Rift. *Scientific Reports*, *8*(1), 1788. https://doi.org/10.1038/s41598-018-20046-4

Schlindwein, V. (2023). H. Bornemann, & S. Amir Sawadkuhi (Eds.), *Reports on polar and marine research, Bremerhaven, Alfred-Wegener-Institut Helmholtz-Zentrum für Polar- und Meeresforschung* (Vol. 781, pp. 121). https://doi.org/10.57738/bzpm_0781_2023.

Song, Y., Nakath, D., She, M., & Köser, K. (2022). Optical imaging and image restoration techniques for deep ocean mapping: A comprehensive survey. *PFG – Journal of Photogrammetry, Remote Sensing and Geoinformation Science*, *90*(3), 243–267. https://doi.org/10.1007/s41064-022-00206-y

Spiess, F. N., Macdonald, K. C., Atwater, T., Ballard, R., Carranza, A., Cordoba, D., Cox, C., Garcia, V. D., Francheteau, J., & Guerrero, J. (1980). East Pacific Rise: hot springs and geophysical experiments. *Science*, *207*(4438), 1421–1433. https://doi.org/10.1126/science.207.4438.1421.

Van Audenhaege, L., Sarrazin, J., Legendre, P., Perrois, G., Cannat, M., Arnaubec, A., & Matabos, M. (2024). Monitoring ecological dynamics on complex hydrothermal structures: A novel photogrammetry approach reveals fine-scale variability of vent assemblages. *Limnology and Oceanography*, *69*(2), 325–338. https://doi.org/10.1002/lno.12486

Wang, M., Lian, S., Xiong, X., Yang, J., Chen, C., & Shi, X. (2024). Assessing the consistency and reliability of the line intercept transect method in coral cover estimation using structure from motion photogrammetry techniques. *Geocarto International*, *39*(1), 2322065. https://doi.org/10.1080/10106049.2024.2322065